

Two Dimensional Photonic Crystal Modes and Resonances in Three-dimensional Structures

Shanhui Fan¹ and J. D. Joannopoulos²

¹Department of Electrical Engineering, Stanford University, Stanford, CA 94305, U. S. A

²Department of Physics and Center for Material Science and Engineering, Massachusetts Institute of Technology, Cambridge, MA 02139, U. S. A

ABSTRACT

We present three-dimensional analysis of two-dimensional guided resonances in photonic crystal slab structures. This analysis leads to a new understanding of the complex spectral properties of such systems. Specifically, we calculate the dispersion diagrams, the modal patterns, and transmission and reflection spectra of these resonances. From these calculations, a key observation emerges involving the presence of two temporal pathways for transmission and reflection processes. Using this insight, we introduce a general physical model that explains the essential features of complex spectral properties. Finally, we show that the quality factors of these resonances are strongly influenced by the symmetry of the modes, and the strength of the index modulation.

INTRODUCTION

Photonic crystal slabs are a particularly important class of photonic crystal structures. A photonic crystal slab consists of a two-dimensionally periodic index contrast introduced into a high-index guiding layer (inset in Figure 1a). These structures support in-plane guided modes that are completely confined by the slab without any coupling to external radiations. These guided modes allow the control of light within the layer at the wavelength scale. Therefore, the slab structure may provide the basic substrate for large-scale on-chip integration of photonic components and circuits. [1-8]

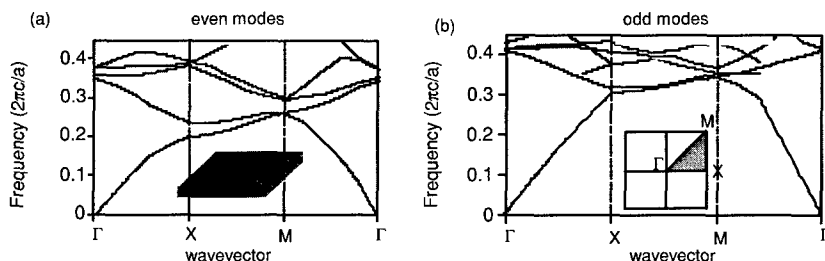


Figure 1. The band structure for (a) even and (b) odd modes in a photonic crystal slab. The structure of the slab is shown in the inset of (a), and consists of a square lattice of air holes with a radius of $0.2a$ introduced into a high-index dielectric slab with a dielectric constant of 12 and a thickness of $0.5a$. Even and odd modes are defined with respect to the mirror parallel to the slab. The gray regions are the continuum of radiation modes. Solid lines outside the gray region are guided modes. Solid lines within the gray region are guided resonances.

In addition to in-plane wave guiding, photonic crystal slabs can also interact with external radiations in complex and interesting ways. Of particular importance here is the presence of guided resonances in the structures. [9-15]. Similar to the guided mode, a guided resonance also has its electromagnetic power strongly confined within the slab. Unlike the guided mode, however, the resonance can couple to external radiations. Therefore, guided resonances can provide an efficient way to channel light from within the slab to the external environment. This property has been exploited in the designs of novel photonic-crystal based light-emitting diodes [11, 16], lasers [17, 18], and directional output couplers [19]. In addition, the guided resonances can significantly affect the transmission and reflection of externally incident light, resulting in complex resonant line shapes that are useful in filter applications. [9][20]

The purpose of this paper is to present a novel analysis of guided resonances in photonic crystal slabs. Our analysis elucidates a variety of complex spectra phenomena associated with these resonances. We compute the dispersion diagrams and the eigen-field distributions of these resonances with a plane-wave band structure computation method. We then perform finite-difference time-domain simulations to determine the transmission and reflection spectra, and to visualize in real time the interaction between the resonances and the incident light. Emerging from these simulations is a key insight that involves the presence of two temporal pathways in the transmission and reflection processes. Based upon this insight, we introduce a general and intuitive theory, which uses only interference and energy conservation arguments, to explain all the complex features in the spectral line shapes. Finally, we analyze the angular and the structural dependence of the guided resonances, and we show the wide ranges of tunability in quality factors for these resonances.

BAND STRUCTURE OF THE GUIDED RESONANCES

Since the spectral features of the guided resonances in a photonic crystal slab will turn out to depend critically on their modal properties, it is helpful to begin our discussion with a brief overview of the band structure properties of these resonances. Throughout this paper, our model system will consist of a square lattice of air holes introduced into a dielectric slab (inset in Figure 1). The thickness of the slab is $0.5a$, and the radius of the holes is $0.2a$, where a is the lattice constant. The dielectric constant of slab is 12, which roughly corresponds to the dielectric constant of Si or GaAs at optical wavelengths. For such a structure, because of the translational symmetries within the plane of the slabs, the physical properties of the slabs can be described by a band diagram that relates the frequencies of all the three-dimensional modes to the in-plane wave vectors [1][2]. The band diagram can be computed by a pre-conditioned conjugate gradient minimization of a Maxwell operator expanded on a plane wave basis [21].

For our model system as shown in the inset of Figure 1a, the band diagram for the even and odd modes are plotted in Figure 1 (a) and (b), respectively. Modes below the light line are bona-fide guided modes with infinite lifetime, in spite of the large index contrast introduced by the air holes. The guided modes above the light line, on the other hand, can couple to radiation modes and possess a finite lifetime. These modes therefore become guided resonances. They are called "guided" since they are closely related to the guided mode bands in a uniform slab, and should therefore retain significant portions of the electromagnetic power within the dielectric slab.

The presence of the air holes in the crystal also generates a discrete translational and rotational symmetry, and thereby dictates the degeneracy of the bands. At most k -points, (except

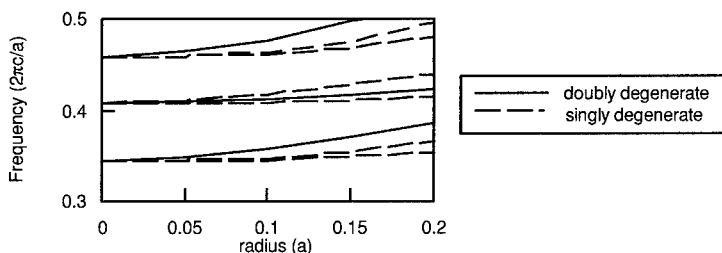


Figure 2. The frequencies of the resonances at Γ as a function of the radius of the holes in the slab. The slab has a dielectric constant of 12 and a thickness of $0.5a$. The modes are four-fold degenerate in the structure without holes. For structures with holes, the four-fold degeneracy is broken, resulting in a pair of doubly degenerate states, and two singly degenerate states.

for the special points Γ , X and M), the bands are singly degenerate. At the Γ point, the point group supports a two-dimensional irreducible representation, allowing for the existence of doubly degenerate states. Therefore, the four-fold degeneracy at the Γ point for a uniform slab splits in the presence of the air holes, as clearly seen in Figure 2, where we plot the frequencies of the resonant modes at Γ as a function of the radius of the holes. As the radius of the holes increases, the modes separate into a pair of doubly degenerate states and two singly degenerate states.

For the crystal structure with $r = 0.20a$, we show the power density distribution of the first resonant band at Γ in Figure 3. The mode is singly degenerate with a frequency $\omega = 0.35 \cdot (2\pi c/a)$. Since any singly degenerate mode should belong to a one-dimensional irreducible representation, the power density distribution of the mode should possess the full symmetry of the lattice. This can be seen in Figure 3(a), which shows the spatial distribution of the power density on a slice parallel to the slab. Also, the resonant nature of this mode is exhibited in Figure 3(b), which shows that the power density is strongly confined within the slab.

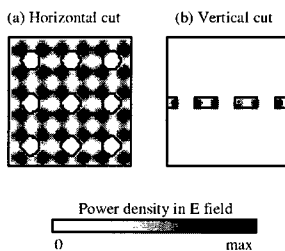


Figure 3. Spatial distribution of the power density in electric fields on (a) a horizontal slice, and (b) a vertical slice, for the lowest-order singly degenerate resonance at Γ . The lines indicate the position of the interface between dielectric and air. The white color represents low intensity and the dark color represents high intensity, as indicated by the color bar at the bottom of the figure.

The band structure computations thus allow us to examine the dispersion, the field distributions, and the symmetry properties of the guided resonances. For a complete understanding of these resonances, however, we must also study their lifetimes, and their interactions with external radiations. These questions will be addressed in the next session by finite-difference time-domain simulations.

TIME-DOMAIN ANALYSIS OF THE GUIDED RESONANCES

Computational methods

The computational domain for our finite-difference time-domain study [22] includes a single unit cell of the crystal. On the top and bottom surfaces of the computational domain, we impose the PML absorbing boundary conditions [23]. For the remaining four surfaces that are perpendicular to the slab, we impose a Bloch periodic boundary condition on the electric fields E :

$$E(r+a) = e^{ik \cdot a} E(r) \quad (1)$$

Here, a is a lattice vector of the square lattice, and k is a wavevector that is parallel to the slab. We note that by Bloch's theorem, k is a conserved quantity in the scattering process.

We generate an incident plane wave by placing a source plane consisting of oscillating dipoles near the top surface of the computational domain. For two dipoles in the plane that are separated by a distance vector r , we set the relative phase between them to be $e^{ik \cdot r}$. Therefore, in combination with the boundary condition as specified in Eq. (1), the source plane generates an incident plane wave with a parallel wavevector component k . In addition, the amplitudes of the dipole moments are set to oscillate at a constant frequency with a Gaussian profile to create a temporal pulse. This computational setup thus allows us to calculate the response functions of the structure at a given k for a wide range of frequencies in a single simulation run. (Notice that this is not a constant incidence angle calculation. At a fixed parallel wavevector k , the incidence angle changes with frequency.)

The transmission and reflection spectra are obtained by first Fourier transforming the recorded time sequence of field amplitudes at their respective monitor points. (We note that monitoring the field amplitudes only at the two monitor points is valid for the frequency range $\omega < 2\pi c/a$, where no diffraction occurs.) The spectra are then normalized with respect to the incident pulse that is calculated in an identical simulation in vacuum without the slab structure. For reflection, the normalization step is preceded by subtracting the incident pulse.

Transmission and reflection spectra

Using the computational setup as described in Section III.1, we calculate the transmission and reflection coefficients at various k -points for the structure as shown in Figure 1. In the case where $k = \hat{x} \cdot 0.2 \cdot 2\pi/a$, the calculated spectra for the s -polarized incident wave are shown in Figure 4. (An s -polarized wave has its electric field perpendicular to the plane of incidence. In this case, the electric field is polarized along the y -direction). The spectra consist of sharp resonant features superimposed upon a smoothly varying background.

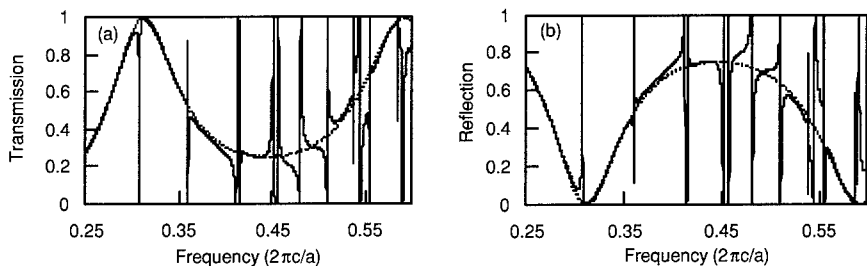


Figure 4. (a) Transmission and (b) reflection spectra. The solid lines are for the photonic crystal structure shown in the inset of Figure 1(a). The dashed lines are for a uniform dielectric slab with a frequency dependent dielectric constant, as defined in Eq. (2), and a thickness of $0.5a$. The incident wave is s -polarized, and has a parallel wavevector $k = 0.2 \cdot 2\pi/a$ along the x -direction.

The background in Figure 4 resembles the Fabry-Perot oscillations when light interacts with a uniform dielectric slab. To clearly see this, we fit the background to the spectra of a uniform slab, which are shown as dashed lines in Figure 4. The uniform slab has the same thickness of $0.5a$ as the crystal, and the light is incident with the same polarization at the same parallel wavevector. The dielectric constant of the uniform slab ϵ_1 , as obtained by the fitting procedure, represents an effective dielectric constant for the photonic crystal. Due to the presence of the holes, such ϵ_1 is a slowly varying function of the frequency. At low frequencies, the wavelength of incident light is large, and ϵ_1 for this polarization approaches the average dielectric constant ϵ_{avg} of the crystal. At higher frequencies, as the incident wave probes more details of the crystal structure, ϵ_1 starts to deviate from ϵ_{avg} . Within the frequency range in Figure 4, i.e. between $0.25 \cdot 2\pi c/a$ and $0.60 \cdot 2\pi c/a$, we have found that a frequency-dependent dielectric constant

$$\epsilon_1(\omega) = -14.16 \cdot \omega^2 + 15.18 \cdot \omega + 7.18 \quad (2)$$

gives a very good fit of the background (Figure 4). The fit here corresponds to varying ω from 10.62 at $\omega = 0.25 \cdot 2\pi c/a$ to 11.5 at $\omega = 0.60 \cdot 2\pi c/a$. (As a comparison, the average dielectric constant for the crystal is 10.6.) Therefore, except for the sharp resonance features, the background of the spectra for the crystal can be adequately accounted for, using the model of a uniform dielectric slab with a frequency-dependent dielectric function.

Line shape analysis

Superimposed upon the smooth background in the spectra for the crystals are sharp resonant features. Such features come from the guided resonances of the slab. In most cases, the line shapes for these resonances are asymmetric and rather complicated. Extensive experimental and theoretical work has been performed for guided resonances in structures with one-dimensionally periodic index variation. [24-31] For structures with two-dimensional periodicity, these resonances have also been studied numerically using the Rigorous Coupled Wave Analysis

(RCWA) method [20], and analytically using vector coupled-mode theory [13][15]. Here, we would like to present a novel analysis from a time-domain perspective. We will observe the important features in the time-domain signatures of the resonances. And, based upon the observation, we will introduce a general and intuitive model to account for the underlying physics.

The transmission and reflection spectra are related to the time-varying fields by a Fourier transformation. It is therefore informative to examine the time dependency of the fields. As an example, we show in Figure 5(a) the electric field amplitude at the transmission monitor point as a function of time steps, for the calculation that gives the spectra shown in Figure 4. The time sequence consists of two distinct stages: an initial pulse, and a tail of long decay.

The presence of these two stages indicates the existence of two pathways in the transmission processes. The first pathway is a direct transmission process, where a portion of the incident energy goes straight through the slab and generates the initial pulse. The Fourier transformation of the initial pulse should account for the background in the transmission spectra. The second pathway is an indirect transmission process, where the remaining portion of the incident energy excites the guided resonances. The power in the resonances then decays slowly out of the structure and produces the long decaying tail. By Fourier transforming the decaying tail, we obtain the typical symmetric Lorentzian line shapes, as shown in Figure 5(b). The analysis of the resonant line shape thus allows us to determine the quality factor Q of the resonance. A few examples of the Q values for this structure are: 360 for the resonance at $\omega = 0.31 \cdot (2\pi c/a)$, and 2500 for the resonance at $\omega = 0.36 \cdot (2\pi c/a)$. The interference between the direct and the indirect pathways, therefore, determine the transmission property. The same observation can be made for the reflected amplitude as well. In solid state and atomic physics, similar interference phenomena are commonly referred to as the Fano resonances [32]. Such temporal interference phenomenon has also been analyzed previously for surface plasmon in metallic thin films [33].

Taking into consideration the interference between these two pathways, we can construct a simple and intuitive model that quantitatively explains the line shape. We express the transmitted amplitude t , and the reflected amplitude r , as follows:

$$t = t_d + f \cdot \frac{\gamma}{i(\omega - \omega_0) + \gamma}, \quad (3)$$

$$r = r_d \pm f \cdot \frac{\gamma}{i(\omega - \omega_0) + \gamma}. \quad (4)$$

Here, t_d and r_d are the direct transmission coefficients, ω_0 and γ are the center frequencies and the widths of the Lorentzian from the resonance, and the factor f is the complex amplitude of the resonant mode.

The plus/minus sign in Eq. (4) corresponds to resonant modes that are even/odd with respect to the mirror plane parallel to the slab. We note that the Lorentzian functions in Eqs. (3) and (4) correspond to the decaying amplitudes of the resonances to the reflection and transmission sides of the slab, respectively. For an even mode, the decaying amplitudes to the two sides of the slab are in phase, while for an odd mode the decaying amplitudes are 180-degree out of phase. Thus, the signs in Eq. (4) are different for modes with different mirror-plane symmetry properties.

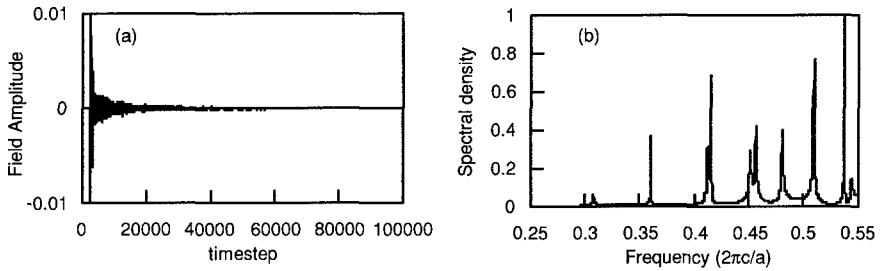


Figure 5. (a) The field amplitude at the monitor point as a function of time step, for the same calculation as shown in Figure 4. Notice the existence of two separate stages: an initial pulse, and a long decaying tail. (b) The Fourier transformation of the amplitude as shown in (a) from time step 20,000 - 100,000. The spectral intensity exhibits Lorentzian line shapes.

The factor f can in fact be determined purely by energy conservation arguments. We note that:

$$|r|^2 + |t|^2 = 1. \quad (5)$$

Moreover, since r_d and t_d are the transmission and reflection coefficients through an uniform slab with the appropriate effective dielectric constant, we should have

$$|r_d|^2 + |t_d|^2 = 1. \quad (6)$$

Constraints (5) and (6) together uniquely determine the factor f . Plugging Eqs (3), (4), and (6) into Eq. (5), we have, for any ω :

$$\begin{aligned} & -2|f|^2 \frac{\gamma^2}{(\omega - \omega_0)^2 + \gamma^2} \\ & = 2|f||t_d \pm r_d| \frac{\gamma}{\sqrt{(\omega - \omega_0)^2 + \gamma^2}} \cos \left(\arg(f) - \arg(t_d \pm r_d) - a \cos \left(\frac{\gamma}{\sqrt{(\omega - \omega_0)^2 + \gamma^2}} \right) \right), \end{aligned} \quad (7)$$

which can only be satisfied if:

$$f = -(t_d \pm r_d). \quad (8)$$

It is interesting to note here that the factor f is independent of the resonant line width γ .

The parameters r_d and t_d represent the background of the spectra. Therefore, as discussed earlier in Section III.2, such parameters can be determined by fitting the background to the response spectra of a uniform slab, as:

$$r_d = \frac{i \frac{k_{z0}^2 - k_{z1}^2}{2k_{z0}k_{z1}} \sin(k_{z1}h)}{\cos(k_{z1}h) - i \frac{k_{z0}^2 + k_{z1}^2}{2k_{z0}k_{z1}} \sin(k_{z1}h)}, \quad (9)$$

$$t_d = \frac{1}{\cos(k_{z1}h) - i \frac{k_{z0}^2 + k_{z1}^2}{2k_{z0}k_{z1}} \sin(k_{z1}h)}, \quad (10)$$

for a plane wave with parallel wavevector k_x , incident from vacuum with a dielectric constant $\epsilon_0 = 1$, through a uniform dielectric slab with a thickness h and a dielectric constant ϵ [34]. The parameters k_{z0} and k_{z1} in Equations (9) and (10) represent the wavevector components along the z -axis in the uniform slab, and are defined as:

$$k_{z0} = \sqrt{\epsilon_0 \frac{\omega^2}{c^2} - k_x^2}, \quad (11)$$

$$k_{z1} = \sqrt{\epsilon_1 \frac{\omega^2}{c^2} - k_x^2} \quad (12)$$

In obtaining Equations (9) and (10), we assume a positive frequency convention, in order to be consistent with the Lorentzian functions that we have chosen for the resonance in Equation (3) and (4).

We note, in particular, when $r_d = 0$, and $t_d = 1$, from Eqs. (3), (4), and (8), the reflection and the transmission coefficients become:

$$t = \frac{i(\omega - \omega_0)}{i(\omega - \omega_0) + \gamma}, \quad (13)$$

and

$$r = \mp \frac{\gamma}{i(\omega - \omega_0) + \gamma}. \quad (14)$$

The line shapes thus become symmetric, and the structure behaves as a narrow-band reflector with a Lorentzian reflectivity line shape. Previously, this scenario was noted by Wang and Magnusson [26]. In the general case when $r_d \neq 0$, on the other hand, the line shape becomes asymmetric. The transmission can vary from 0% to 100% within a very narrow frequency range. A small shift in the resonant frequency may therefore lead to a drastic change in the response function. This effect may be exploited in the design of optical sensors and switches.

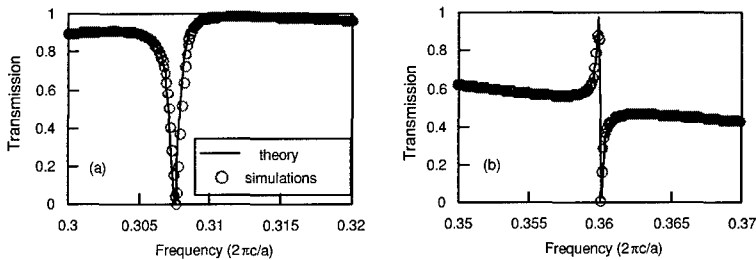


Figure 6. Comparison of theory and simulations. The empty circles in (a) and (b) are numerical results taken from Figure 5(a), which corresponds to the two lowest-frequency resonances. The solid lines are theoretical predictions from Eqs. (3), (8), (9) and (10). The parameters of the theory for the two resonances are: (a) $\omega_0 = 0.3076 \cdot 2\pi c/a$, $\gamma = 4.191 \cdot 10^{-4} \cdot 2\pi c/a$; (b) $\omega_0 = 0.3601 \cdot 2\pi c/a$, $\gamma = 7.2483 \cdot 10^{-5} \cdot 2\pi c/a$.

We compare our theoretical predictions, as defined by Eqs. (3), (4), (8), (9) and (10), to the numerical results for the first two resonances shown in Figure 5. (Both of these resonances are even.) The frequency ω and the width γ of each resonance are determined from the simulations. The only fitting parameter here is the effect dielectric constant ϵ_1 , which we take from Equation (2). The theoretical results thus obtained are shown as solid lines in Figure 6. The theory agrees completely with the numerical simulations.

Wavevector dependency of the resonances

To explore the wavevector and polarization dependency of the resonances, we performed calculations at different values of k_x , for an incident wave that is either *s*- or *p*- polarized. (The *s*-polarization has the electric field perpendicular to the plane of incidence, while the *p*-polarization has the magnetic field perpendicular to the plane of incidence). We determine the position and the width of the resonances by Fourier transforming the decaying tail, as discussed earlier in section III.3. The results are summarized in Figure 7(a), where we show the frequencies of the resonances as a function of k_x . Incident waves with different polarizations excite different resonances, since the two polarizations possess different symmetries with respect to *yz*-mirror plane.

We note that, in Figure 7(a), some of the bands do not continue to the Γ point. In other words, certain resonances at Γ do not couple to either polarization of the incident wave. A closer examination of Figure 7(a) reveals that all these uncoupled resonances are singly degenerate. Previously, this effect was observed experimentally by Pacradoni et al [14], and discussed theoretically by Paddon and Young [13], and by Ochiai and Sakoda [25]

To further explore the wavevector dependency of the resonance, in Figure 7(b) we plot the quality factors of the resonances as a function of k_x , for the four lowest bands in Figure 7(a). For bands with different symmetry properties, the behavior of the quality factors is very different. The *Q* factors approach a constant as k_x vanishes for the modes that connect to the doubly degenerate states at Γ . For the modes that connect to the singly degenerate states, on the other hand, the *Q* factors of the modes diverge. The calculation clearly demonstrates that the symmetry of the modes can significantly influence the photon lifetime of the resonances.

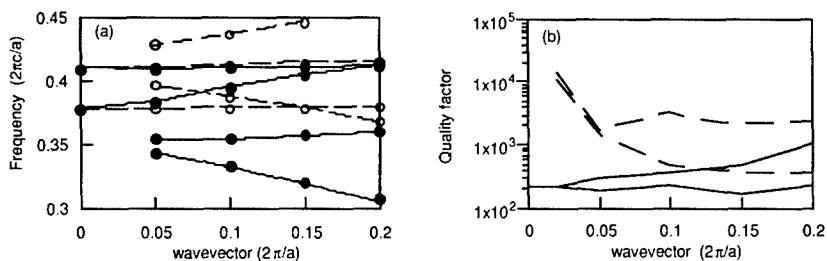


Figure 7. (a) The frequencies of the resonances as a function of wavevector, for the structure as shown in the inset of Figure 1a, as determined from the time-domain simulations. The solid circles correspond to the resonances that are excited by the p-polarized incident waves, the empty circles correspond to the resonances that are excited by the s-polarized incident waves. Notice that some of the bands do not continue to Γ , indicates the existence of uncoupled states at Γ . (b) The quality factor as a function of wavevector, for the four lowest bands in (a). The solid lines correspond to modes that connect to the doubly degenerate state at Γ point. The broken lines correspond to modes that connect to the singly degenerate state at Γ point.

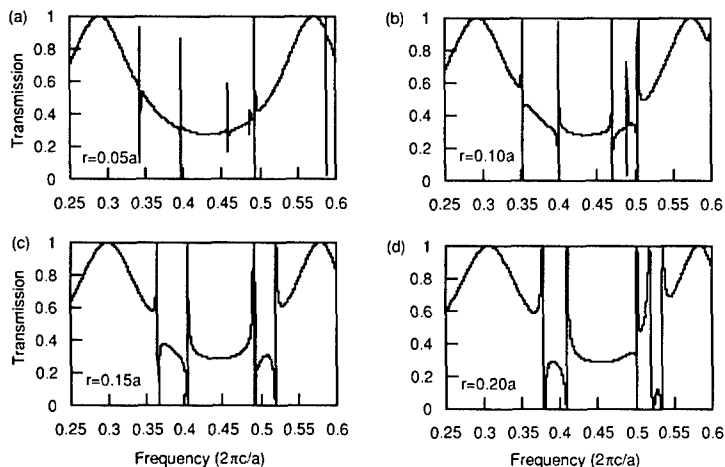


Figure 8. The transmission spectra at normal incidence, for crystal slab structures with a radius of (a) $0.05a$; (b) $0.10a$; (c) $0.15a$, and (d) $0.20a$. All the structures have a thickness of $0.5a$, and a dielectric constant of 12.

Radius dependence of the resonance.

In addition to symmetry related effects, the lifetime of the resonances is also strongly influenced by the radius of the holes. At the limit where the radius of the holes approaches zero, the Q factor for all the resonances should diverge, since the resonances asymptotically become real guided modes. To demonstrate this effect, we plot in Figure 8 the transmission spectra at normal incidence for four different structures with the radius varying from $0.05a$ to $0.20a$. The spectral feature for the resonances indeed becomes sharper as the radius becomes smaller. For the lowest-order resonances, the Q factor varies from approximately 5000 at $r = 0.05a$, to 213 at $r = 0.20a$. At a larger radius, the Q-factor should be even lower.

The tunability of the quality factor with respect to the radius of the holes is important for LED and laser applications. For photonic-crystal resonant-cavity LED structures, optimal efficiency occurs when the line width of the resonances become comparable to the line width of the emitter [35]. On the other hand, for a laser structure, a high-Q resonance is typically desirable for threshold reduction. Therefore, as we have demonstrated in this paper, photonic crystal slab structures are very versatile, and can be specifically tailored for different light emitting applications.

SUMMARY

In summary, we present a three-dimensional frequency and time-domain analysis of resonances in photonic crystal slab structures. These resonances are strongly confined with the dielectric slab, and yet at the same time are coupled to radiation modes. For external light incident upon these slabs, the transmission and reflection spectra are strongly modified by the presence of these resonances. The line shapes exhibit complex asymmetric characteristics. We show that all the complexities in the line shapes can be accounted for with a simple analytic model describing the interference between direct transmission (or reflection), and the exponential decaying amplitudes of the resonances. We also demonstrate that the quality factors of these resonances are strongly influenced by the symmetry of the modes, and the radius of the holes.

ACKNOWLEDGMENT

This work was supported in part by the Material Research Science and Engineering Center program of the National Science Foundation under Award No. DMR-9400334.

REFERENCES

1. S. Fan, P. R. Villeneuve, J. D. Joannopoulos, and E. F. Schubert, *Phys. Rev. Lett.* 78, 3294-7 (1997).
2. S. G. Johnson, S. Fan, P. R. Villeneuve, and J. D. Joannopoulos and L. A. Kolodzeski, *Phys. Rev. B* 60, 5751-8 (1999).
3. O. Painter, T. Vuckovic, and A. Scherer, *J. Opt. Soc. Am. B* 16, 275-85 (1999).
4. T. Baba, N. Fukaya, and J. Yonekura, *Electron. Lett.* 35, 654-5 (1999).
5. S. Kuchinsky, D. C. Allan, N. F. Borrelli, and J. -C. Cotteverte, *Opt. Commun.* 175, 147 (2000).
6. S. Y. Lin, E. Chow, S. G. Johnson, J. D. Joannopoulos, *Opt. Lett.* 25, 1297-9 (2000).

7. H. Benisty et al, *Appl. Phys. Lett.* 76, 531-3 (2000).
8. A. Chutinan and S. Noda, *Phys. Rev. B* 62, 4488-92 (2000).
9. M. Kanskar, P. Paddon, V. Pacradouni, R. Morin, A. Busch, J. F. Young, S. R. Johnson, J. MacKenzie and T. Tiedje, *Appl. Phys. Lett.* 70, 1438-40 (1997).
10. P. R. Villeneuve, S. Fan, S. G. Johnson, and J. D. Joannopoulos, *IEE Proceedings: Optoelectronics* 145, 384 (1998).
11. M. Boroditsky, R. Vrijen, T. F. Krauss, R. Coccioli, R. Bhat, and E. Yablonovitch, *J. Lighwave Technol.* 17, 2096-112 (1999).
12. V. N. Astratov, I. S. Chushaw, R. M. Stevenson, D. M. Whittaker, M. S. Skolnick, T. F. Krauss, and R. M. De la Rue, *J. Lighwave Technol.* 17, 2050-8 (1999).
13. P. Paddon and J. F. Young, *Phys. Rev. B* 61, 2090-2101 (2000).
14. V. Pacardoni, W. J. Mandeville, A. R. Crown, P. Paddon, J. F. Young and S. R. Johnson, *Phys. Rev. B.* 62, 4204-7 (2000).
15. A. R. Cowan, P. Paddon, V. Pacradouni, and J. F. Young, *J. Opt. Soc. Am. A* 16, 1160-70 (2001).
16. A. A. Erchak, D. J. Ripin, S. Fan, J. D. Joannopoulos, E. P. Ippen, G. S. Petrich, and L. A. Kolodzeski, *Appl. Phys. Lett.* 78, 563-5 (2001).
17. M. Meier, A. Mekis, A. Dodabalapur, A. Timko, R. E. Slusher, J. D. Joannopoulos, *Appl. Phys. Lett.* 74, 7-9 (1999).
18. M. Imada, S. Noda, A. Chutinan, T. Tokuda, M. Murata and G. Sasaki, *Appl. Phys. Lett.* 75, 316-8 (1999)
19. A. Mekis, A. Dodabalapur, R. E. Slusher, and J. D. Joannopoulos, *Opt. Lett.* 25, 942-4 (2000).
20. S. Peng and G. M. Morris, *J. Opt. Soc. Am. A* 13, 993-1005 (1996).
21. J. D. Joannopoulos, R. D. Meade and J. N. Winn, "Photonic crystals: molding the flow of light" (Princeton University Press, Princeton, 1995).
22. For a review on finite difference time domain methods, see K. S. Kunz and R. J. Luebbers, "The finite difference time domain methods for electromagnetics", (CRC press, Boca Raton, 1993); A. Taflove and S. C. Hagness, "Computational Electrodynamics: the finite-difference time-domain method", (Artech House, Boston, 2000).
23. J. P. Berenger, *J. Computational Physics* 114, 185-200 (1994).
24. S. S. Wang and R. Magnusson, *Appl. Phys. Lett.* 61, 1022-24 (1992).
25. T. Ochiai and K. Sakoda, *Phys. Rev. B* 63, 125107-1 (2001).
26. S. S. Wang and R. Magnusson, *Opt. Lett.* 19, 919-921 (1994).
27. A. Sharon, D. Rosenblatt, A. A. Friesem, *Opt. Lett.* 21, 1564-6 (1996).
28. T. Tamir and S. Zhang, *J. Opt. Soc. Am A* 14, 1607-1616 (1997)
29. S. M. Norton, T. Erdogan and G. M. Morris, *J. Opt. Soc. Am. A* 14, 629-639 (1997).
30. S. M. Norton, G. M. Morris and T. Erdogan, *J. Opt. Soc. Am A* 15, 464-472 (1998).
31. G. Levy-Yurista and A. A. Friesem, *Appl. Phys. Lett.* 77, 1596-1598 (2000).
32. U. Fano, *Phys. Rev.* 124, 1866-77 (1961).
33. R. V. Andalaro, H. J. Simon, and R. T. Deck, *Appl. Opt.* 33, 6340-7 (1994).
34. P. Yeh, "Optical waves in layered media", (John Wiley & Sons, New York, 1988).
35. S. Fan, P. R. Villeneuve, and J. D. Joannopoulos, *IEEE J. Quantum Electron.* 36, 1123-30 (2000).